UDC 54.01:542.8:544.2:548.3 doi: 10.15407/hftp16.01.039

I.M. Shcherbatiuk [1], T.V. Lisnycha [1], K.D. Pershina [1, 2]

IMPACT OF THE TiO_2 POLYMORPHIC MODIFICATIONS AND CITRIC ACID AMOUNT ON THE PARTICLE SIZE AND CRYSTALLITE FORMATION OF LITHIUM-CONTAINING TITANIUM OXIDES UNDER THE MELTING ROUTE

[1] V.I. Vernadsky Institute of General and Inorganic Chemistry of National Academy of Sciences of Ukraine
32/34 Academician Palladin Aven., Kyiv, 03142, Ukraine, E–mail: katherinepersh@gmail.com
[2] National Technical University of Ukraine "Igor Sikorsky Kyiv Polytechnic Institute"
37 Berestejskyi Ave., Kyiv, 03056, Ukraine

The presented work aimed to synthesize and melt lithium- containing titanium oxides in the citric acid media, and to determine the impact of the ratio of TiO_2 polymorphic modifications and citric acid amount on the particle size and crystallite formation. New approaches for changing particle and crystallite size were performed based on the post-synthetic melting treatment in the solid citric acid of the Li- containing TiO_2 powders. The X-ray powder diffraction analysis detected the main TiO_2 polymorphs phases (anatase, rutile, Ti_6O_{11}, Ti_3O_5, $Li_{0.026}TiO_2$, and lithium titanium oxide (2.7/1.3/4) in all samples prepared via orthotitanic acid alkaline hydrolysis and under the melting route in citric acid media. There was a correlation between the ratio of citric acid in the melting mixture and crystallite size in ending products. The maximum anatase crystallite size (10372 nm) was detected in the samples prepared in media with a large surplus of citric acid. The total pore volume (V_{total}) was calculated from the volume of nitrogen adsorbed converted to liquid at a pressure close to $P/P_0 = 1$. All samples were found to involve two kinds of pores: micropores with approx. 1÷2 nm radius, and mesopores with approx. 10÷29 nm radius. The samples' SEM analysis also detected the size of the two kinds of particles in all samples. Increasing amounts of citric acid lead to increasing amounts of particles with size < 100 nm in the presence of small amounts of large-scale (> 900 nm) particles. The maximum pore and particle size were detected after melting treatment TiO_2 polymorphs in media with a large surplus of citric acid. It was proposed a scheme of crystallite formation in the presence of Magnéli phases and reductants from the thermal decomposition of citric acid.

***Keywords**: titanium oxides, polymorphic modifications, orthotitanic acid alkaline hydrolysis, citric acid, melting treatment, pore size, particle size*

INTRODUCTION

During the last decades, considerable attention has been paid to electrochemical energy storage devices with high energy and high power densities, because of their opportunities to use in powering electric vehicles and portable electronic devices. Rechargeable lithium- and sodium-based batteries are amongst the most promising candidates in terms of energy density [1]. However, the achievement of high power density is hindered by kinetic problems of the electrode materials. For achieving a high rate capability of such batteries, rapid ionic and electronic diffusion is necessary. Many research works have focused on enhancing mixed conduction by doping the electrode materials with foreign atoms [2, 3] or by admixing electronically conductive phases (electronic wiring through carbon, conducting polymers, Ag, heavy metal oxides, *etc*.) [4–7]. Another way to solve the kinetic problems of the electrode materials is the use of nano-architectured electrodes consisting of metal oxides combined with metals as a current collector or the use of porous TiO_2 thin films [8, 9]. To optimize the device's performances, a proper design of the electrodes is necessary to balance the different charge storage mechanisms. The nanoscopic network structure is composed of a dense net of metalized mesopores that allow both Me^+ and e^- to migrate. This network, with a mesh size of about 10 nm, is superimposed by a similar net on the microscale, formed by the composite of the mesoporous particles and the conductive admixture for realization of the intercalation electrode. The power of this concept is demonstrated by the synthesis of a mesoporous $TiO_2 : RuO_2$ nanocomposite, which shows a superior high-rate capability when used as the anode material for lithium batteries [4, 9]. As

result, nanostructuring the electrode materials is one of the strategies to enable fast kinetics with shorter diffusion distances for Li ions, improving the charge transfer kinetics and material accessibility [10, 11]. Mesoporous nano-structured materials are particularly interesting because of their high surface area, offering more metal insertion channels, pores and pathways for fast diffusion of metal ions [12]. The performance of an electrode depends strongly on the preparation process and its final homogeneity. Microsized mesoporous sphere-like materials are optimal for the electrode preparation due to high packing density and the it ability to attain uniform and compact layers. Above all, TiO_2 is a promising material to be used in the intercalation electrode, due to its high abundance, low toxicity and cost, high discharge voltage plateaus and structural stability during Li-ion insertion/extraction [12–14]. Between some polymorph forms of TiO_2 the polymorph anatase has been extensively studied because of its ability to store a high amount of lithium, with a theoretical capacity of 335 mAh g^{-1} [4]. However, the bulk form suffers from solid-state diffusion limitation and low electron conductivity in pure anatase. On other hand different polymorphs of TiO_2-based nanostructured anode materials with large surface-area-to-volume ratios to maintain stable contact with the electrolyte, short Li^+ ion diffusion paths, facile strain relaxation upon battery cycling and rise conductivity due to percolation effects between polymorphs of TiO_2 [15]. Such properties of TiO_2 completed the target of the work. It was to detect the impact of the ratio of TiO_2 polymorph modifications and citric acid amount on the size and crystallite formation of lithium-containing titanium oxides during the melting route.

EXPERIMENTAL

Materials.

Preparation of series of Li^+-doped TiO_2 nanoparticles. TiO_2 samples (with size 90–230 nm) were synthesized using alkaline hydrolysis of $TiCl_4$ by LiOH solutions. The samples were dried at 150 °C for 10 h with further thermal treatment at 350–470 °C in the air for 4, 26, 40, and 45 hours. The starting materials for preparing TiO_2 polymorphs were the aqueous solutions of titanium tetrachloride (98 % $TiCl_4$) without further purification. The synthetic method for the preparation of orthotitanic acid ($Ti(OH)_4$) and mixture of anatase and rutile is illustrated in Fig. 1. The synthesis consists of two stages: the first stage is hydrolysis of the water solution of titanium tetrachloride with Li_2SO_4 and LiOH; the second stage consists of drying and thermal treatment to receive stable content of anatase-rutile ratio.

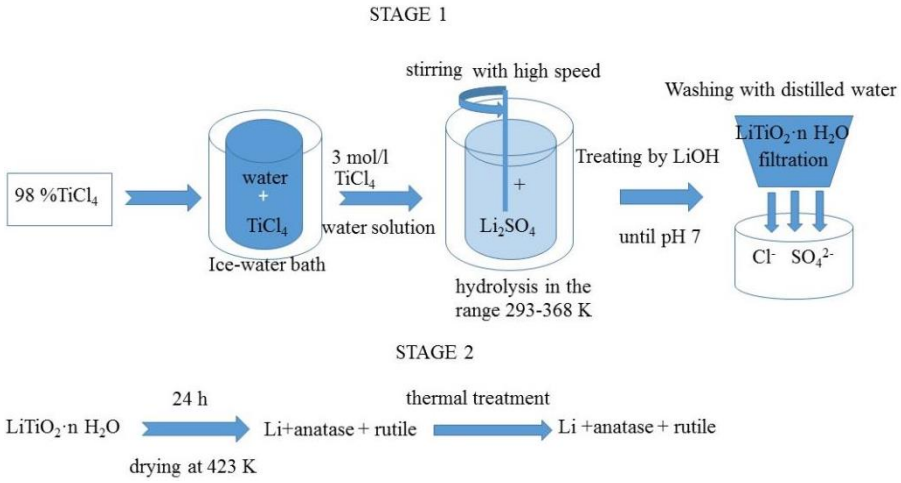

Fig. 1. Principle scheme of the lithium anatase-rutile mixture preparation via orthotitanic acid

Molten treatment by citric acid of the lithium – anatase-rutile mixture. The molten route anatase–rutile–citric acid was used to change the nanoscopic network structure of powders. After the samples prepared according to the scheme of synthesis (Fig. 1), they had been melt in solid citric acid media(Table 1).

Table 1. Conditions of the sample preparation

Sample No.	Citric acid mass ratio	Treatment temperature for the first stage, °C	Treatment time for the first stage, hours	Treatment time for the first stage, °C	Treatment time for the second stage, hours
1	1 : 0	-	-	-	-
2	1 : 2	230	3	470	2
3	1 : 3	230	3	520	2
4	1 : 4	230	3	520	2

Characterization of materials. The structural investigation and X-ray powder diffraction analysis were performed on a (CuK_a radiation (l ¼ 0.15418 nm) and a Bragg 2θ configuration. The intensities of X-ray reflections were measured in the range 2θ = 10–80° with a step width of 0.02, the X-ray beam probed a sample area of ~ 50 mm^2. The phase content and crystallite size estimations were performed use Match 3.0 software. Average crystallite size calculated from selected peaks/lines: 932.4 Å. From the line broadening of the corresponding X-ray diffraction peaks and using the Scherrer's formula, the crystallite size estimated by:

$$L = \frac{K\lambda}{\beta Cos\Theta} \quad (1)$$

where L is the average crystallite size in nm, λ is the wavelength of the X-ray radiation (0.154056 nm for copper lamp), K is a constant usually taken as 0.9, β is the line width at half-maximum height in radians, and θ is the diffracting angles [16]. The Scherrer constant used in calculation of crystallite size was 0.94. A fraction of rutile phase in each sample was determined via the usually accepted quantitation method. This method consisted of measuring the relative XRD intensities of the anatase (101) (d = 0.3520 nm) and rutile (110) (d = 0.3247 nm), and then the fraction of rutile phase was calculated using Spurr equation [17]:

$$FR = \frac{1}{1+0.8[I_A(101)/I_R(110)]} \quad (2)$$

where FR - the mass fraction of rutile in the powder, I_A and I_R are X-ray integrated intensities of the (101) reflection of anatase and (110) reflection of rutile, respectively.

Specific surface areas and pore size distributions for the synthesized samples were calculated from nitrogen adsorption/desorption curves (NOVA 2200e, Quantachrome, USA) using the Nova Win 2.0 software. Before measurements, the samples were vacuum-treated overnight at 120 °C. The total surface area of the materials S_{total} was calculated by the Brunauer-Emmet-Teller method (BET). The total pore volume (V_{total}) was calculated from the volume of nitrogen adsorbed converted to liquid at a pressure close to P/P_0 = 1. To acquire the volume and radii of mesopores ($V_{meso,}$ R_{meso}), Barrett-Joyner-Halenda (BJH) were used. The average pore radii (R_{pore}) was determined from the total pore volume (V_{total}) of the materials and its specific surface area (S_{total}) by equation $R_{pore} = 2V_{total}/S_{total}$. The micropore volume ($V_{micro}$) was calculated by subtracting the value of V_{meso} from V_{total}. Pore radii distributions were obtained from isotherms in terms of the density functional theory (DFT).

The thermal behavior of the precursors was examined by means of thermogravimetric (TG and DTG) and differential thermal analysis (DTA) using a Q-1500D derivatograph (MOM, Hungary) at atmospheric pressure in air (heating rate 10 °/min, probe mass ~ 0.1 g, temperature up to 600 °C).

RESULTS AND DISCUSSION

The X-ray diffraction patterns in Fig. 2 illustrate the effect of acids concentration on the phase formation. Theoretical and experimental works show that the synthesis of the different TiO_2 polymorphs strongly depends on the precursor and the synthesis conditions e.g. ligand concentration, acid or base media, temperature, synthesis duration, *etc*. Due to structure similarities, the different complexes led to a certain TiO_2 structure. In summary, it could be able to say, that the surface properties of TiO_2 are changed or modified so that the intermediate product's total Gibbs free energy surface favors the formation of a certain TiO_2 polymorphs [18]. A high charge density at the surface can strongly decrease the surface energy [19] and lead to

metastable and/or unexpected TiO_2 phases. Therefore, it is possible to synthesize very small rutile crystals as well as larger anatase crystals, which are thermodynamically unstable. For such purpose, using the melting route with citric acid is one of the routes that combine opportunities to control the acidity and receiving of intermediates by changing the TiO_2 - citric acid ratio.

The composition of the synthesized TiO_2 and TiO_2 - $HOC(CH_2CO_2H)_2$ with different acid ratios have four TiO_2 polymorphs and two $Li_xTi_yO_z$ compounds with small amount of anatase and rutile phases relatively Ti_6O_{11} and Ti_3O_5 phases in all studied samples (Fig. 2, Tables 2, 3). $Li_{0.026}TiO_2$ has additional reflections as in the materials, which could be indexed with the same structure as the pristine anatase TiO_2 (space group $I4_1/$ amd, a = 3.7919, c = 9.7979) albeit with different lattice parameters (Table 3). The work observed that electrochemical Li insertion should lead to two two-phase regions: first the well-established anatase/Li-titanate (α/β) coexistence, and second the newly observed phase coexistence between Li-titanate and the Li_1TiO_2 phase (β/γ) [20]. Based on that it could be possible to assume a similarity in lithium incorporation in anatase phases during electrochemical processes and lithium anatase-rutile mixture preparation via orthotitanic acid alkaline hydrolysis. Such similarity allows for the thermodynamic impact of particle sizes of anatase, which takes part in crystallite growth provided by the Gibbs free energy (per mole inserted Li - ions) for mixing two phases in a bulk material [20]. It doesn't give opportunities for crystallite and particles growth. On other hand in the TiO_2/lithium titanium oxide (2.7/1.3/4) systems crystallite size increases from 40 to 105 nm as a function of the annealing temperature [21]. All these sizes are lower than crystallite size detected in studied objects (Table 4). The more promising polymorphs impacted on crystallite size can be Ti_6O_{11} and Ti_3O_5 polymorphs (Table 2, Fig. 2).

Table 2. TiO_2 polymorphs in the samples fixed on XDR spectra

TiO_2 polymorphs	***d* [Å]**	**Entry No.**
Anatase	3.5142; 2.4305; 2.3781; 2.3324; 1.8921; 1.7471; 1.6997; 1.6663; 1.4933; 1.4807; 1.3389	96-901-5930; 96-900-9087; 96-720-6076; 96-500-0224; 96-900-8215; 96-900-8216; 96-900-8217
Rutile	3.2466; 2.4869; 2.2960; 2.1869; 2.0542; 1.6877; 1.6663; 1.6242; 1.4807; 1.4529; 1.3611; 1.3468	96-900-9084; 96-900-7433; 96-900-1682; 96-900-7532; 96-900-4142; 96-901-5663; 96-410-2356; 96-900-4143; 96-900-4144; 96-900-4145
Ti_6O_{11}	3.5046; 3.4932; 3.4668; 3.4440; 3.3430; 3.2978; 2.0511; 2.4991; 2.4824; 2.4819; 2.4798; 2.4368; 2.3742; 2.2993; 2.2978; 2.0632; 1.8923; 1.7466; 1.6910; 1.6833; 1.6622; 1.6280; 1.6204; 1.4803; 1.4506; 1.3577; 1.3368; 1.3027; 1.2635; 1.2698; 1.2506	96-152-1096
Ti_3O_5	3.5420; 3.4480; 3.3345; 3.3295; 3.3029; 3.1456; 2.8494; 2.8163; 2.6841; 2.6641; 2.6031; 2.4699; 2.4366; 2.4045; 2.3786; 2.3747; 2.3663; 2.3592; 2.3403; 2.3379 2.2118; 2.1952; 2.1657; 2.1360; 1.1519 1.4370; 1.4081; 1.3780; 1.3640; 1.3594; 1.3422; 1.2994	96-231-0726
$Li_{0.026}Ti\ O_2$	3.5216; 2.4302; 2.3743; 2.3348; 1.8959; 1.6983; 1.6694; 1.4948; 1.4816; 1.3631; 1.3406; 1.2774; 1.2850; 1.2529; 1.1872; 1.1739; 1.1674; 1.1626; 1.0599; 1.0453; 1.0166	96-412-4519
Lithium titanium oxide (2.7/1.3/4)	2.3671; 2.0500; 1.4496; 1.1836; 1.0250	96-101-0898

Table 3. The main Crystal systems of TiO_2 polymorphs detected in samples

TiO_2 polymorphs	**Crystal system**	**Space group**	**Unit cell, A**	**Calc. density, g/cm^3**
Anatase	tetragonal	$I4_1$/ amd (141)	*a* = 3.78420 *b* = 9.51460	3.894
Rutile	tetragonal	$P4_2$/ mnm	*a* = 4.5922 *b* = 2.9574	4.233
Ti_6O_{11}	monoclinic	$C1_2$/m 1 (12)	*a* = 9.94600 *b* = 3.74400 *c* = 20.99400	3.942
Ti_3O_5	monoclinic	$C1_2$/m 1 (12)	*a* = 9.75200 *b* = 3.80200 *c* = 9.44200	4.245
$Li_{0.026}Ti\ O_2$	tetragonal	$I4_1$/ amd (141)	*a* = 3.79190 *c* = 9.79790	3.894

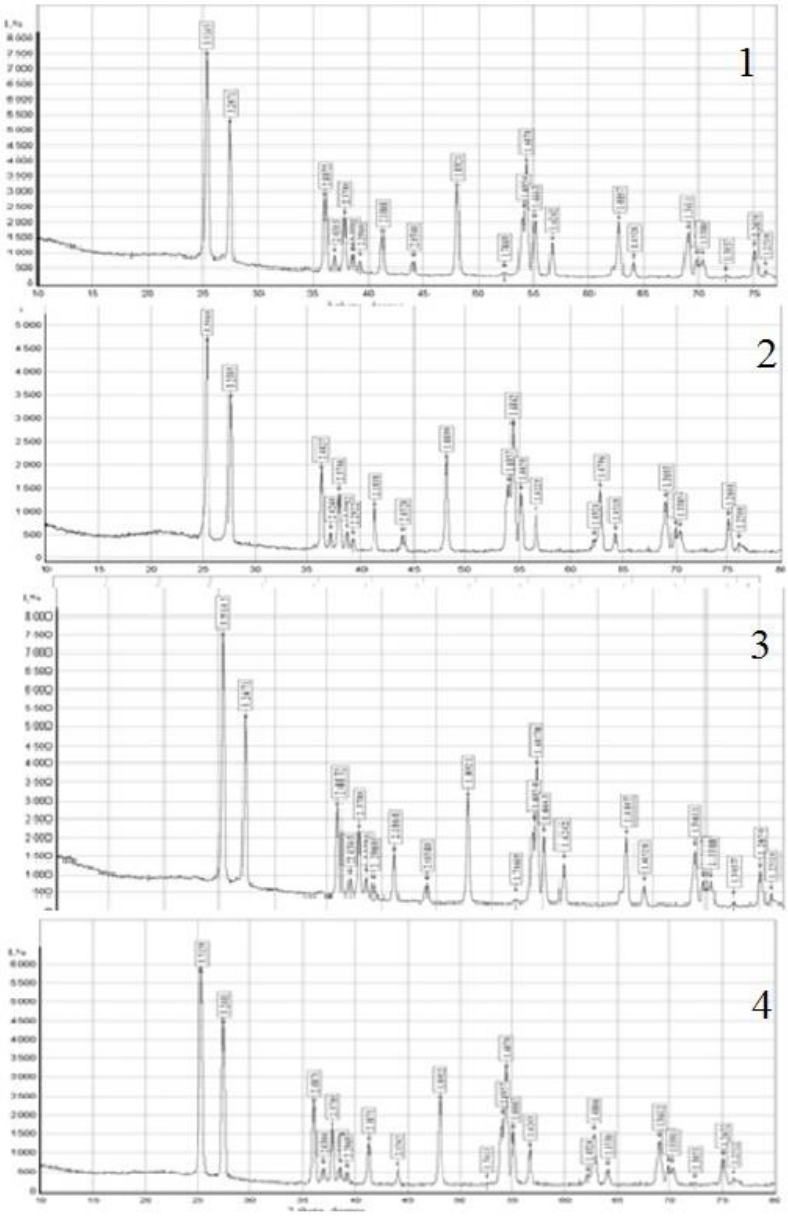

Fig. 2. X-ray diffraction patterns of the studied samples (the numeration is according to Table 1)

Ti_6O_{11} and Ti_3O_5 phases have 'nonstoichiometric' structures e.g., TiO_{n-2} and/or TiO_n and so-called Magnéli phases, which have the formula $Ti_{2n}O_{2n-1}$, where n = 4, ..., 10. There is research where Ti_3O_5 and TiO_2 (anatase) were observed clearly without any signs of TiO_2 (rutile) in XRD-diffractograms [22]. It was reported that such Ti_3O_5 form of TiO_{2-x}/TiO_2-based heterostructures could be formed at the temperature of 400 °C, which is suitable for the formation of Ti_3O_5 with TiO_2 (anatase)-intergrowths [23] at very different formation conditions. When TiO_2 is used as the titanium source, reductants like carbon, hydrogen, certain active metals (e.g. Ti, Si, Mg, Al, or Ca), and organic acids are used to remove oxygen and prepare different titanium suboxides, even the polymorphism of the same titanium suboxide. Besides, titanium suboxide single crystals can be grown in presence of oxygen in the reactor atmosphere. On another hand $Ti_{2n}O_{2n-1}$ is mixed-valence compounds with two Ti^{3+} ($3d^1$ electronic configuration) and (n = 2) Ti^{4+} ($3d^0$) ions. The presence of both Ti^{3+} and Ti^{4+} ions provides several possible configurations of cations in the crystal, leading to various charge-ordered states and promoting the formation of crystallites with large sizes [22, 23].

According calculation the growth of crystallite sizes of anatase in studied samples have such tendency: pure anatase< pure rutile < sample 2 < sample 1< sample 3< sample 4. The tendency in changing sizes of crystallites of the rutile is the same one, but the sizes are much lower (Tables 4, 5). With the exception of sample 3 all samples have correlation with behavior of anatase in presence of Magnéli phases. Rutile is the thermodynamic stable phase, but for small particle sizes anatase become the dominating phases. Summary of results obtained from the X-ray diffraction patterns and BET surface area of all the samples are shown in Table 4.

Table 4. Crystallite size, average pore size and surface area of samples

Sample	Crystallite size* (nm)	Average pore size, nm	Surface area (m^2 g^{-1})	
			This work	Literaturre
1	91.46 (R). 376.05 (A)	1.75; 30	8.51	-
2	83.04 (A) 87.84 (R)	1.6; 28.3	5.54	-
3	89.79 (R). 357.10 (A)	1.5; 19.6	7.22	-
4	98.08 (R) 10372 (A)	1.6; 28.4	6.33	-
Anatase	16.3 (A)	1.7	6.09	5.90 [27]
Rutile	42.7 (R)	5.5	31.41	50

*Calculated from XRD data using Eq. (1). A denotes anatase and R denotes rutile

The reason for this is the Gibbs free energy G_0 of the system consisting of a bulk G_{bulk} and a surface term $G_{surface}$:

$$G_0 = G_{bulk} + G_{surface}\,. \quad (3)$$

In nanoscaled materials, the system is more dependent on the surface term while materials with a bigger particle size are dominated by the bulk term. Rutile has the lowest G_{bulk} value, but anatase have lower $G_{surface}$ values. Therefore, the three polymorphs have a thermodynamic crossover at a certain particle size leading to stable anatase particles at small crystallite size and stable rutile particles at bigger crystallite sizes [24]. Rutile is more stable than anatase for a particle size > 14 nm [23, 25]. In a later study, they postulated that anatase is thermodynamically stable at sizes 35 nm and the crystal structure strongly depends on the synthesis method. It seems that anatase to be more stable for small nanoparticles. But the anatase crystallite sizes of sample 4 can't be classified as nanocrystalline TiO_2 powders (Table 4). It could be possible to explain based on a thermodynamic approach that uses surface, edge, and vertex energies, calculated from first principles, to make predictions about the shapes and energetics of large crystallites, using surface and edge energies in the presence of

Magnéli phase titanium oxides [26]. The active impact of the anatase phase in the formation of surface properties of samples is confirmed by close data of surface area in pure anatase [27] and studied samples (Table 4). In all object with equilibrium or lit bit larger amount of anatase phase the size of crystallites of anatase is more than crystallites of rutile phases (Table 4). It could be connected with the Magnéli phase titanium oxides properties. In Ti_nO_{2n-1}, an oxygen deficiency in every n^{th} layer leads to shear planes in the crystal structure. At the shear planes, the two-dimensional chains of octahedra share a face to accommodate the deficiency in oxygen with the formation of large crystallites. The conditions of such changes can be realized under the thermal treatment of anatase or rutile phases in the presence of reductants or pressure in the temperature range of 20–400 °C [23]. The Ti_3O_5 is the main phase formed on the anatase surface, and Ti_6O_{11} is formed on rutile.

Table 5. Ratio of the Titanium polymorphs in the samples calculated from X-ray diffraction patterns

Sample	Ratio of the titanium polymorphs				
	Anatase : Rutile	**Rutile : Ti_6O_{11}**	**Anatase : Ti_3O_5**	**Rutile : Ti_3O_5**	**$Li_{0.026}TiO_2$: lithium titanium oxide (2.7/1.3/4)**
1	1 : 1	1 : 1.5	8 : 1	1 : 1	7 : 1
2	1.1 : 1	1 : 2	4 : 1	1 : 1.3	8 : 1
3	1.1 : 1	1 : 2	6.4 : 1	1 : 1.3	7 : 1
4	1 : 1.1	1 : 1.4	10 : 1	1 : 1	7 : 1

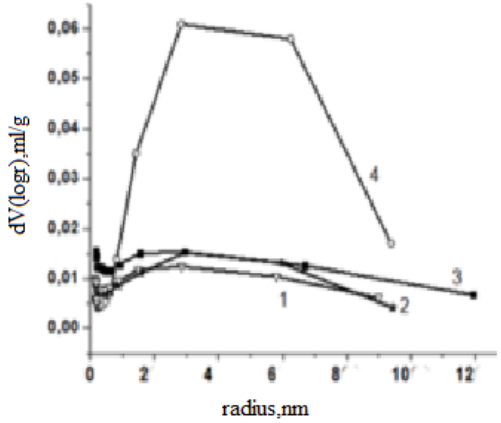

Fig. 3. Changes of pore size in the studied samples (the numeration is according Table 1)

The results of the XRD analysis are in good agreement with pore sizes (Fig. 3) and SEM images (Fig. 4). All samples have two main pore sizes: < 2 nm (micropores) and 2 - from 10 to 29 nm (mezopores) (Table 4, Fig. 3). The maximum pore size was detected in sample 4 (Fig. 3). The SEM analysis of the samples also detected the two kinds of the particles size in the samples after synthesis of the lithium – anatase - rutile mixture preparation via orthotitanic acid and after melting treatment in citric acid media (Fig. 4). Increasing amount of citric acid lead to increasing amount of particles with size < 100 nm in the presence of small amount of large scale particles. On the other hand, thermal treatment in a reducing environment produces a number of defects in the TiO_2 crystal structure, including oxygen vacancies (V_o). The increasing number of V_o alters the Ti and O ratio, resulting in the formation of different suboxides (i.e., Magnéli compounds). Magnéli phases usually form from TiO_2 according to the following reaction [23]:

$nTiO_2 + V_O \rightarrow Ti_nO_{2n-1}$.

An increasing citric acid amount in a melting mixture two times raises the number of reductants (products of citric acid decomposition and CO_2) [28, 29] in 20 % with further polymerization of these products in temperature range 210÷490 °C and formation of carbon structures at temperature 490–500 °C [30] (Figs. 5, 6).

Such intermediates could take part of the Magnéli phase formation:

$$n(TiO_2)_s + \text{organic reductants (s)} =$$

$$= Ti_nO_{2n-1} + H_2O\,(g) + CO\,(g)$$

$$n(TiO_2)_s + CO(g) = Ti_nO_{2n-1} + CO_2\,(g).$$

This could explain the huge rise of crystallite sizes in the case of citric acid's significant surplus due to the formation of many reductants in synthetic mixtures (Fig. 7).

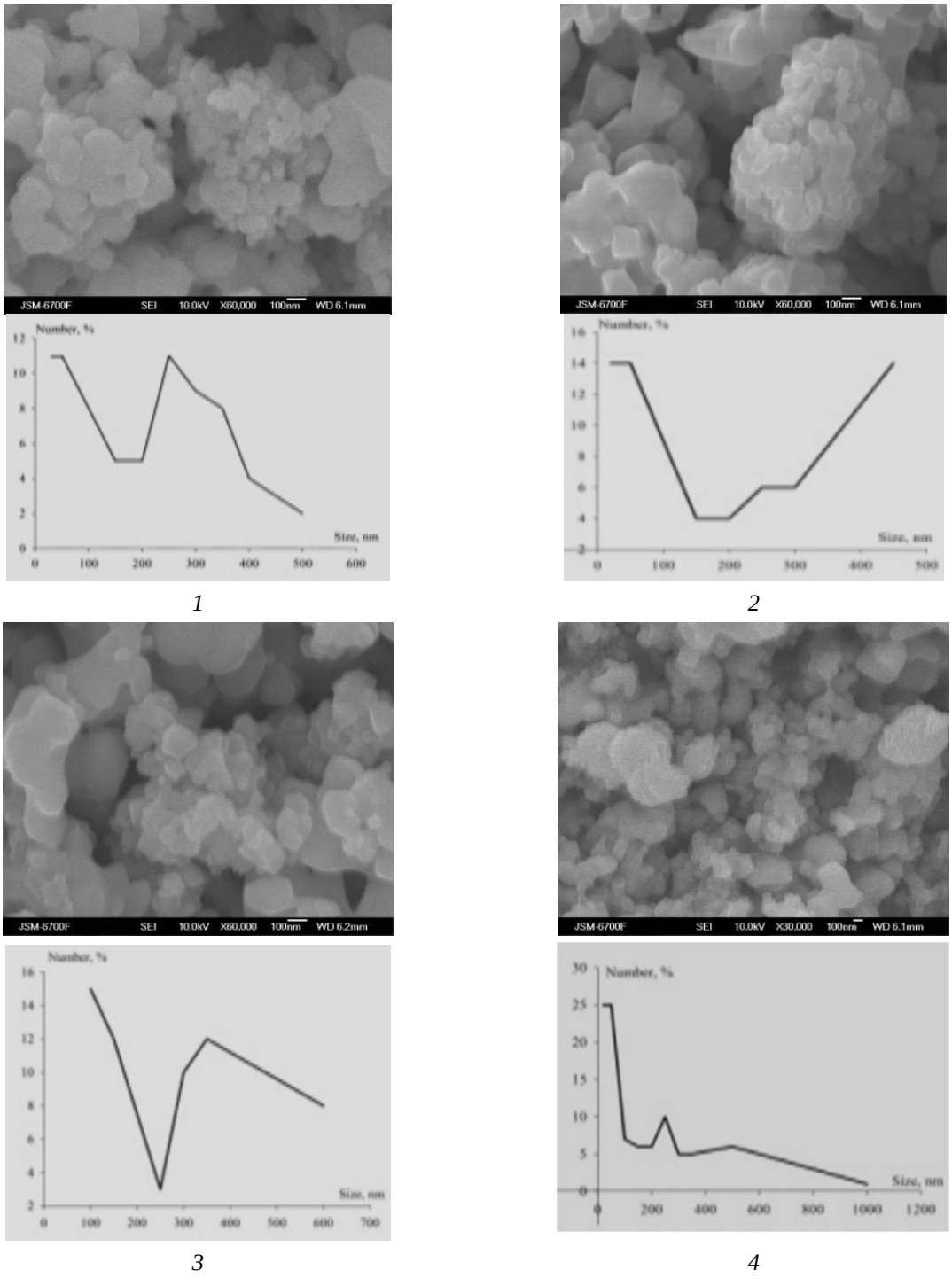

Fig. 4. SEM images of the samples: *1* – $TiO_{2\ primary}$ (the lithium anatase-rutile mixture preparation via orthotitanic acid); *2* – TiO_2 + Citrate Acid 1 : 2; *3* – TiO_2 + Citrate Acid 1 : 3; *4* – TiO_2 + Citrate Acid 1 : 4

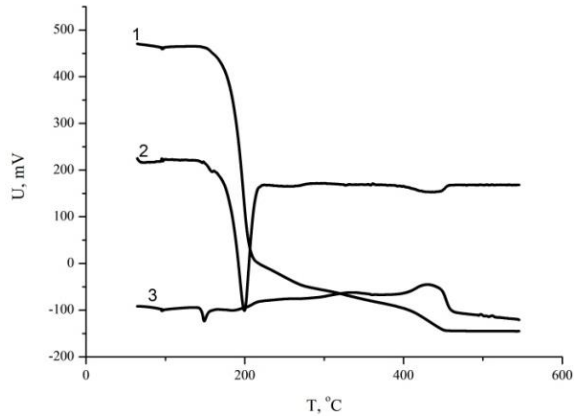

Fig. 5. TG (*1*), DTG (*2*) and DTGA (*3*) data of the mixture 2 (Table 1)

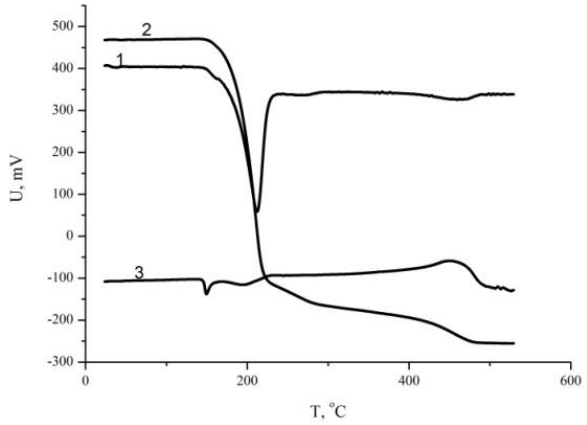

Fig. 6. TG (*1*), DTG (*2*) and DTGA (*3*) data of the mixture 4 (Table 1)

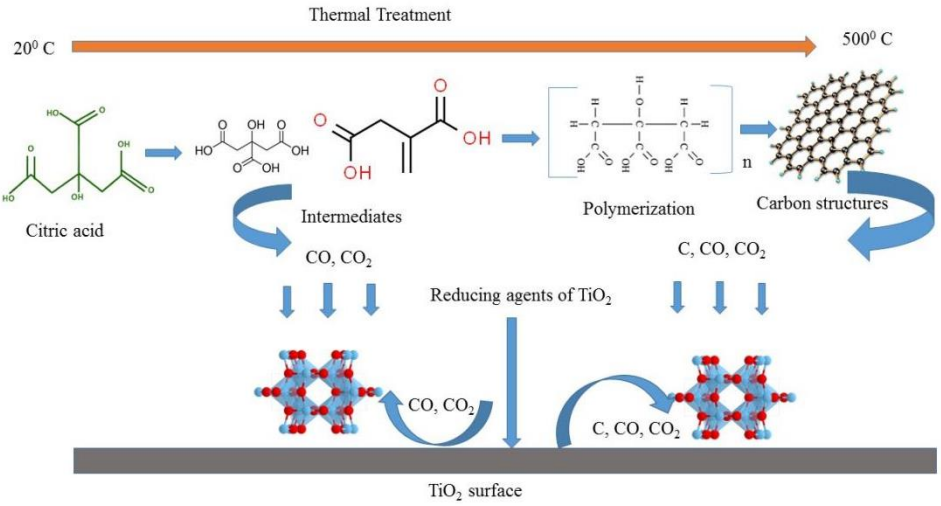

Fig. 7. Scheme of the reductant's and Magnéli phases formation in presence of citric acid on TiO_2 surface

CONCLUSIONS

The lithium-containing titanium oxides were synthesized using ortho-titanic acid alkaline hydrolysis with further post-synthetical melting treatment with solid citric acid. The composition of the synthesized TiO_2 and TiO_2 - $HOC(CH_2CO_2H)_2$ with different acid ratios have four TiO_2 polymorphs and two $Li_xTi_yO_z$

compounds with small amount of anatase and rutile phases relatively Ti_6O_{11} and Ti_3O_5 phases in all studied samples. Detected structures specialties of $Li_{0.026}TiO_2$ give us to assume similarity in lithium incorporation in anatase phases during electrochemical processes and lithium anatase-rutile mixture preparation via orthotitanic acid alkaline hydrolysis and absence of the thermodynamic opportunities for crystallite and particles growth. It was detected a correlation between the ratio of citric acid in the melting mixture and crystallite size in ending products. The maximum anatase crystallite size (10372 nm) was in the samples received from large surplus of citric acid. All samples were found to involve two kinds of pores: micropores with approx. 1÷2 nm radius, and mesopores with approx.10÷29 nm radius. The samples' SEM analysis also detected the size of the two kinds of particles in all samples. Increasing amounts of citric acid lead to increasing amounts of particles with size < 100 nm in the presence of small amounts of large-scale (> 900 nm) particles. Based on XDR analysis, TG, DTG, and TGA data the scheme of crystallite formation in the presence of Magnéli phases and the appearance of reductants during the thermal decomposition of citric acid was proposed.

ACKNOWLEDGEMENTS

The authors would like to express their deep appreciation to the National Academy of Sciences of Ukraine (NASU) for the financial support our work "Strategy for creating electrode materials of Na- and Li-ions current sources using molten compositions (SR N_0 0122U200365).

Вплив поліморфних модифікацій TiO_2 та кількості лимонної кислоти на розмір частинок та утворення кристалітів в літійвмісних оксидах титану при плавленні

І.М. Щербатюк, Т.В. Ліснича, К.Д. Першина

Інститут загальної та неорганічної хімії імені В.І. Вернадського Національної академії наук України
просп. Академіка Палладіна, 32/34, Київ, 03142, Україна, katherinepersh@gmail.com
Національний технічний університет України «Київський політехнічний інститут імені Ігоря Сікорського»
просп. Берестейський, 37, Київ, 03056, Україна

Ця робота спрямована на синтез та плавлення літійвмісних оксидів титану в середовищі лимонної кислоти й визначення впливу співвідношення поліморфних модифікацій TiO_2 та кількості лимонної кислоти на розмір частинок та утворення кристалітів. Нові підходи до зміни розміру частинок і кристалітів були реалізовані на основі постсинтетичного плавлення в твердій лимонній кислоті порошків TiO_2, що містять Li. Рентгеноструктурний аналіз виявив основні поліморфні фази TiO_2 (анатаз, рутил, Ti_6O_{11}, Ti_3O_5, $Li_{0,026}TiO_2$ та оксититанату літію (2.7/1.3/4) у всіх зразках, отриманих шляхом лужного гідролізу орто-титанової кислоти та плавленням в середовищі лимонної кислоти. Була виявлена кореляція між співвідношенням лимонної кислоти в суміші для плавлення та розміром кристалітів у кінцевих продуктах. Максимальний розмір кристалітів анатазу (10372 нм) виявлений у зразках, що отримані у середовищах із великим надлишком лимонної кислоти. Загальний об'єм пор (Vtotal) розраховувався з об'єму азоту, перетвореного в рідину при тиску, близькому до $P/P_0 = 1$. Було встановлено, що в усіх зразках присутні два типи пор: мікропори з приблизним радіусом 1÷2 нм та мезопори з приблизно 10÷29 нм. СЕМ аналіз зразків також виявив розміри двох типів частинок у всіх зразках, що призводить до збільшення кількості частинок з розміром < 100 нм у присутності невеликих кількостей великомасштабних (> 900 нм) частинок. Максимальний розмір пор і частинок виявлено після обробки поліморфів TiO_2 плавленням у середовищі з великим надлишком лимонної кислоти. Запропоновано схему утворення кристалітів у присутності фаз Магнелі та відновників термічного розкладання лимонної кислоти.

***Ключові слова**: оксиди титану, поліморфні модифікації, лужний гідроліз орто-титанової кислоти, лимонна кислота, обробка плавленням, розмір пор, розмір частинок*

REFERENCES

1. Li F., Wei Z., Manthiram A., Feng Y., Ma J., Mai L. Sodium-based batteries: from critical materials to battery systems. *J. Mater. Chem. A.* 2019. **7**(16): 9406.
2. Wu Y.P., Rahm E., Holze R. Effects of heteroatoms on electrochemical performance of electrode materials for lithium ion batteries. *Electrochim. Acta.* 2002. **47**(21): 3491.
3. Qian H., Ren H., Zhang Y., He X., Li W., Wang J., Hu J., Yang H., Sari H.M.Kh., Chen Yu, Li X. Surface doping vs. bulk doping of cathode materials for lithium-ion batteries: a review. *Electrochem. Energy Rev.* 2022. **5**(4): 2.
4. Guo Y.G., Hu Y.S., Sigle W., Maier J. Superior electrode performance of nanostructured mesoporous TiO_2 (anatase) through efficient hierarchical mixed conducting networks. *Adv. Mater.* 2007. **19**(16): 2087.
5. Deng H., Lin L., Ji M., Zhang S., Yang M., Fu Q. Progress on the morphological control of conductive network in conductive polymer composites and the use as electroactive multifunctional materials. *Prog. Polym. Sci*. 2014. **39**(4): 627.
6. Zhang Y., Tao L., Xie C., Wang D., Zou Y., Chen R., Wang Y., Jia Ch., Wang Sh. Defect engineering on electrode materials for rechargeable batteries. *Adv. Mater.* 2020. **32**(7): 1905923.
7. Zhang A., Liang Y., Zhang H., Geng Z., Zeng J. Doping regulation in transition metal compounds for electrocatalysis. *Chem. Soc. Rev.* 2021. **50**(17): 9817.
8. Ellis B.L., Knauth P., Djenizian T. Three-dimensional self-supported metal oxides for advanced energy storage. *Adv. Mater.* 2014. **26**(21): 3368.
9. Hallot M., Boyaval C., Troadec D., Huve M., Karroubi L.B., Patnaik S.G., ...&Lethien, C. Three-Dimensional TiO_2 Film Deposited by ALD on Porous Metallic Scaffold for 3D Li-Ion Micro-Batteries: A Road towards Ultra-High Capacity Electrode. *J. Electrochem. Soc.* 2022. **169**(4): 040523.
10. Dylla A.G., Henkelman G., Stevenson K.J. Lithium insertion in nanostructured TiO_2 (B) architectures. *Acc. Chem. Res.* 2013. **46**(5): 1104.
11. Berger T., Monllor-Satoca D., Jankulovska M., Lana-Villarreal T., Gomez R. The electrochemistry of nanostructured titanium dioxide electrodes. *ChemPhysChem.* 2012. **13**(12): 2824.
12. Liu R., Duay J., Lee S.B. Heterogeneous nanostructured electrode materials for electrochemical energy storage. *Chem. Commun.* 2011. **47**(5): 1384.
13. Dambournet D. Cationic vacancies in anatase (TiO_2): synthesis, defect characterization, and ion-intercalation properties. *Acc. Chem. Res.* 2022. **55**(5): 696.
14. Liu Z.G., Du R., He X.X., Wang J.C., Qiao Y., Li L., Chou S.L. Recent progress on intercalation-based anode materials for low-cost sodium-ion batteries. *ChemSusChem.* 2021. **14**(18): 3724.
15. Bresser D., Paillard E., Binetti E., Krueger S., Striccoli M., Winter M., Passerini S. Percolating networks of TiO2 nanorods and carbon for high power lithium insertion electrodes. *J. Power Sources.* 2012. **206**: 301.
16. Muniz F.T.L., Miranda M.R., Morilla dos Santos C., Sasaki J.M. The Scherrer equation and the dynamical theory of X-ray diffraction. *Acta Crystallographica Section A: Foundations and Advances.* 2016. **72**(3): 385.
17. Zanatta A.R. A fast-reliable methodology to estimate the concentration of rutile or anatase phases of TiO_2. *AIP Adv.* 2017. **7**(7): 075201.
18. Wang Y., Feng T., Li X., Li L. Thermochemistry of nano-phased titanium dioxides relevant to energy application: A Review. *Chem. Thermodyn. Therm. Anal.* 2022. **5**: 100033.
19. Hanaor D.A., Sorrell C.C. Review of the anatase to rutile phase transformation. *J. Mater. Sci.* 2011. **46**: 855.
20. Wagemaker M., Borghols W.J., Mulder F.M. Large impact of particle size on insertion reactions. a case for anatase $Li_x TiO_2$. *J. Am. Chem. Soc.* 2007. **129**(14): 4323.
21. Picquart M., Escobar-Alarcon L., Torres E., Lopez T., Haro-Poniatowski E. Structural study of lithium titanium mixed oxides prepared by sol-gel process. *J. Mater. Sci.* 2002. **37**: 3241.
22. Malik H., Sarkar S., Mohanty S., Carlson K. Modelling and synthesis of Magnéli Phases in ordered titanium oxide nanotubes with preserved morphology. *Sci. Rep.* 2020. **10**(1): 8050.
23. Xu B., Sohn H.Y., Mohassab Y., Lan Y. Structures, preparation and applications of titanium suboxides. *RSC Adv.* 2016. **6**(83): 79706.
24. Castro R.H., Wang B. The hidden effect of interface energies in the polymorphic stability of nanocrystalline titanium dioxide. *J. Am. Ceram. Soc.* 2011. **94**(3): 918.
25. Ranade M.R., Navrotsky A., Zhang H.Z., Banfield J.F., Elder S.H., Zaban A., Borse P.H., Kulkarni S.K., Doran G.S., Whitfield H.J. Energetics of nanocrystalline TiO_2. *Proceedings of the National Academy of Sciences.* 2002. **99**(suppl_2): 6476.
26. Barnard A.S., Erdin S., Lin Y., Zapol P., Halley J.W. Modeling the structure and electronic properties of TiO_2 nanoparticles. *Phys. Rev. B.* 2006. **73**(20): 205405.
27. Raj K., Viswanathan B. Effect of surface area, pore volume and particle size of P25 titania on the phase transformation of anatase to rutile. *Indian J. Chem.* 2009. **48A**: 1378.

28. Barbooti M.M., Al-Sammerrai D.A. Thermal decomposition of citric acid. *Thermochim. Acta.* 1986. **98**: 119.
29. Chen Y., Deng Y., Zhang H., Wang L., Ma J. A novel and simple route to synthesis nanocrystalline titanium carbide via the reaction of titanium dioxide and different carbon source. *Mater. Sci. Appl.* 2011. **2**(11): 1622.
30. Winter J.H., Tate B.E. Polymerization of itaconic acid and derivatives. In: *Fortschritte der Hochpolymeren-Forschung*. (Springer Berlin Heidelberg, 1967). pp. 214–232.

Received 17.07.2024, accepted 05.03.2025